Journal of Electrical Engineering & Technology (2019) 14:817–824
https://doi.org/10.1007/s42835-018-00068-8

ORIGINAL ARTICLE

Dual Band RCS Reduction Using Modulated Grooves in A Conducting Plane

Sangsu Lee[1] · Heejae Jun[2] · Kyung-Young Jung[3] · Hosung Choo[4] · Ic-Pyo Hong[5] · Yong Bae Park[1]

Received: 27 August 2018 / Revised: 31 October 2018 / Accepted: 21 November 2018 / Published online: 8 January 2019
© The Korean Institute of Electrical Engineers 2019

Abstract
An electromagnetic boundary-value problem of modulated grooves in a conducting plane is rigorously solved based on the Fourier transform, eigenfunction expansion, and mode matching method. Radar cross section (RCS) of the modulated grooves is represented in a series form and calculated while varying depth, width, and period of the grooves to investigate scattering characteristics of dual band RCS reduction.

Keywords Radar cross section · Mode matching method · Modulated grooves

1 Introduction

Recently, there have been extensive studies on the extraordinary optical transmission through subwavelength slits surrounded by surface grooves [1–5]. The enhanced optical transmission through the slits surrounded by grooves on the surface results from the surface plasmon polariton (SPP) resonance [6]. In fact, the SPP modes are the special transverse magnetic surface wave modes propagating along the interface between two media with positive and negative permittivities in the optical region. The SPP modes are decaying evanescently in the direction perpendicular to the interface. The SPP-like modes can be also sustained by a perfect electric conductor even in the micro/millimeter wave regimes when its surface is periodically corrugated [7–9]. The SPP-like modes are also referred to as a spoof SPP or designer SPP because they are bound electromagnetic surface waves that mimic the SPP modes in optical region [7, 9]. A previous experimental study showed that the excitation of the SPP-like modes over the interface of the grooved conducting plane can reduce reflectivity at X band in a case of normal incidence [11]. Electromagnetic scattering from the rectangular groove in a conducting plane has also been investigated [12–14]. However, the previous studies have analyzed electromagnetic scattering by the rectangular groove in terms of the geometry of the groove and they have not taken into account the effects of the SPP-like modes. Therefore, it is of great interest to rigorously solve the electromagnetic scattering from the grooves in a conducting plane in the viewpoint of the SPP-like modes and to analyze the relationship between the excitation of the SPP-like modes and the scattering characteristic. In addition, a previous study has shown that the SPP-like modes can be generated at multiple frequencies on the conductor surface with modulated grooves using a number of in-depth simulations [15]. Therefore, it is significantly meaningful to rigorously analyze the excitation of the SPP-like modes with respect to the grooves geometries and to study the feasibility of the reduction of the reflection at multiple

✉ Yong Bae Park
yong@ajou.ac.kr

Sangsu Lee
lss1507@ajou.ac.kr

Heejae Jun
hjjun@moasoftware.co.kr

Kyung-Young Jung
kyjung3@hanyang.ac.kr

Hosung Choo
hschoo@hongik.ac.kr

Ic-Pyo Hong
iphong@kongju.ac.kr

1 Department of Electrical and Computer Engineering, Ajou University, Suwon, South Korea

2 MOASOFT Corporation, Seoul, South Korea

3 Department of Electronic Engineering, Hanyang University, Seoul, South Korea

4 School of Electronic and Electrical Engineering, Hongik University, Seoul, South Korea

5 Department of Information and Communication Engineering, Kongju National University, Gongju, South Korea

SPP-like mode resonance frequencies. Lately, radar-absorbing material (RAM) [16], design of mount shape [17], and plasma on scatterers [18–20] have been studied for radar cross section (RCS) reduction, and the RCS reduction is considerably crucial in stealth technology.

In this paper, we solve an electromagnetic boundary-value problem of the modulated grooves in an infinite conducting plane based on mode matching method. The eigenfunction expansion and the Fourier transform are used to represent the electromagnetic field in each region in terms of the discrete and continuous modes. The boundary conditions are enforced to obtain a simultaneous equation. RCS of the modulated grooves in a conducting plane is represented in the series form and calculated by using surface equivalence theorem [10]. Computation is performed to illustrate the behaviors of the reflection with respect to the grooves geometries. In order to validate our formulation, simulation results of Microwave Studio (MWS) of CST and FEKO are compared with our results. Also, the relationship between the excitation of the SPP-like mode and the reduction of reflection is discussed in detail.

2 Field Analysis

Let us assume that a plane wave is TM-polarized and incident on an infinite rectangular conducting plane with two different periodic grooves on the surface, as shown in Fig. 1. The grooves in each period have different sizes, which appears to be a modulated geometry with different depths, widths, and periods. A time convention of $e^{j\omega t}$ is suppressed throughout the analysis. The permittivity and permeability in region I and II are ϵ_1, μ_1, $\epsilon_2^{(i)}$, and $\mu_2^{(i)}$. Superscript (i) indicates the i-th groove from the left. In region I, the incident and reflected fields are

$$H_y^{i,r}(x,z) = e^{-jk_x x \pm jk_z z}, \tag{1}$$

$$E_x^{i,r}(x,z) = \left(\mp\frac{k_z}{\omega\epsilon_1}\right) e^{-jk_x x \pm jk_z z}, \tag{2}$$

where $k_x = k_1 \sin\theta_i$, $k_z = k_1 \cos\theta_i$, and $k_1 = \omega\sqrt{\mu_1\epsilon_1}$.

The scattered field can be represented based on Fourier transform as [12, 21]

$$H_y^s(x,z) = \frac{1}{2\pi}\int_{-\infty}^{\infty} \tilde{H}_y^s(\zeta) e^{j\zeta x - j\kappa_1 z} d\zeta, \tag{3}$$

$$E_x^s(x,z) = \frac{1}{2\pi}\int_{-\infty}^{\infty} \frac{\kappa_1}{\omega\epsilon_1} \tilde{H}_y^s(\zeta) e^{j\zeta x - j\kappa_1 z} d\zeta, \tag{4}$$

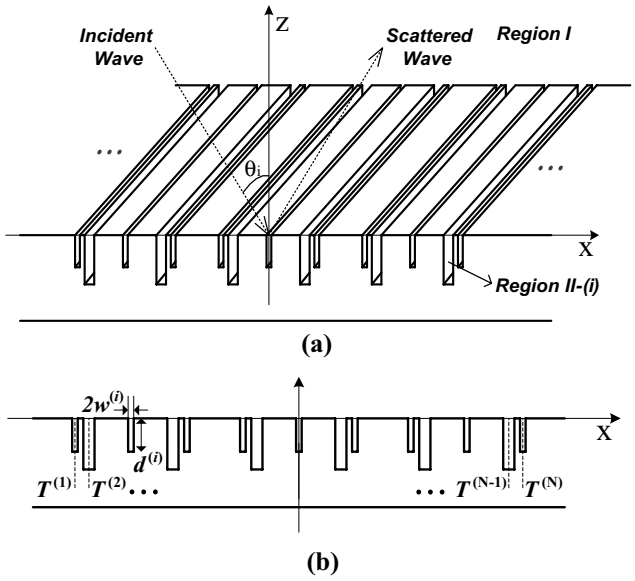

Fig. 1 **a** The proposed geometry with modulated grooves in an infinite conducting plane and **b** the front view of the structure

where $\kappa_1 = \sqrt{k_1^2 - \zeta^2}$. In region II, the electromagnetic field can be represented in the sum of discrete modes and takes the form of:

$$H_y^{\mathrm{II}-(i)}(x,z) = \sum_{m=0}^{\infty} A_m^{(i)} \cos\left[a_m^{(i)}\left(x + w^{(i)} - T^{(i)}\right)\right] \times \cos\left[\chi_m^{(i)}\left(z + d^{(i)}\right)\right], \tag{5}$$

$$E_x^{\mathrm{II}-(i)}(x,z) = \sum_{m=0}^{\infty} \frac{A_m^{(i)}}{j\omega\epsilon_2^{(i)}} \cos\left[a_m^{(i)}\left(x + w^{(i)} - T^{(i)}\right)\right] \times \left(\chi_m^{(i)}\right) \sin\left[\chi_m^{(i)}\left(z + d^{(i)}\right)\right], \tag{6}$$

where $A_m^{(i)}$ is a modal coefficient of i-th groove ($i = 1, \ldots, N$), $a_m^{(i)} = \frac{m\pi}{2w^{(i)}}$, $\chi_m^{(i)} = \sqrt{\left(k_2^{(i)}\right)^2 - \left(a_m^{(i)}\right)^2}$, and $k_2^{(i)} = \omega\sqrt{\mu_2^{(i)}\epsilon_2^{(i)}}$. The boundary conditions are enforced to obtain the simultaneous equation for modal coefficients. The tangential electric field continuity is applied at the interface between region I and II ($z = 0$)

$$E_x^i(x,0) + E_x^r(x,0) + E_x^s(x,0) = \begin{cases} E_x^{\mathrm{II}-(i)}(x,0) & -w^{(i)} + T^{(i)} < x < w^{(i)} + T^{(i)} \\ 0 & \text{elsewhere} \end{cases}. \tag{7}$$

Taking the inverse Fourier transform $\int_{-\infty}^{\infty}(\cdot)e^{-j\zeta x}dx$ to (7) yields

$$\tilde{H}_y^s(\zeta)=\sum_{i=1}^{N}\frac{\epsilon_1}{\epsilon_2^{(i)}}\sum_{m=0}^{\infty}A_m^{(i)}\left(\chi_m^{(i)}\right)\sin\left(\chi_m^{(i)}d^{(i)}\right)\frac{\zeta}{\kappa_1}e^{-j\zeta T^{(i)}}\times\frac{\left[(-1)^m e^{-j\zeta w^{(i)}}-e^{j\zeta w^{(i)}}\right]}{\zeta^2-\left(a_m^{(i)}\right)^2}. \tag{8}$$

Afterwards, the tangential magnetic field continuity is applied at the same interface

$$H_y^i(\mathrm{x},0)+H_y^r(\mathrm{x},0)+H_y^s(\mathrm{x},0)=H_y^{\mathrm{II}-(i)}(\mathrm{x},0)-w^{(i)}+T^{(i)}<x<w^{(i)}+T^{(i)}. \tag{9}$$

By substituting (8) into (9) and applying the orthogonality of trigonometric functions to (9), we can get the simultaneous equation:

$$\begin{aligned}&j2k_x e^{-jk_x T^{(l)}}\frac{\left[(-1)^s e^{-jk_x w^{(l)}}-e^{jk_x w^{(l)}}\right]}{k_x^2-\left(a_s^{(l)}\right)^2}\\&-\frac{j}{2\pi}\sum_{i=1}^{N}\frac{\in_1}{\in_2^{(i)}}\sum_{m=0}^{\infty}A_m^{(i)}\left(\chi_m^{(i)}\right)\sin\left(\chi_m^{(i)}d^{(i)}\right)\\&\times\int_{-\infty}^{\infty}\frac{\zeta^2}{\kappa_1}e^{-j\zeta(T^{(i)}-T^{(i)})}\frac{\left[(-1)^m e^{-j\zeta w^{(i)}}-e^{j\zeta w^{(i)}}\right]}{\zeta^2-\left(a_m^{(i)}\right)^2}\\&\times\frac{\left[(-1)^s e^{j\zeta w^{(l)}}-e^{-j\zeta w^{(l)}}\right]}{\zeta^2-\left(a_s^{(l)}\right)^2}\\&=A_s^{(l)}w^{(l)}\gamma_m^s\cos\left(\chi_s^{(l)}d^{(l)}\right)\delta_{ms}\delta_{il}.\end{aligned} \tag{10}$$

$$\gamma_m^s=\begin{cases}2 & m=s=0\\1 & \text{otherwise}\end{cases}. \tag{11}$$

To calculate the integral from in (10), we use Gaussian quadrature integration. Using (10), it is possible to obtain the modal coefficient $A_m^{(i)}$ in each groove.

3 Numerical Results and Discussion

Three dimensional RCS is defined as [10]:

$$\sigma_{3-\mathrm{D}}=\lim_{r\to\infty}4\pi r^2\frac{\left|H_y^r+H_y^s\right|^2}{\left|H_y^i\right|^2}. \tag{12}$$

Since calculating the integral form of H_y^s in (3) is not easy and time-consuming, we introduce equivalent electric and magnetic surface current densities on the surface of the conducting plane ($z=0$). First, on the parts consisting of a perfect electric conductor, equivalent electric surface current density can be defined at $z=0$ as:

$$\overrightarrow{J_s}=2\hat{n}\times\overrightarrow{H_t^i}, \tag{13}$$

where subscription t indicates the tangential component. On the other hand, the rest parts on the surface of the proposed geometry, equivalent magnetic surface current density is defined at $z=0$ as:

$$\vec{M}_s^{\mathrm{II}-(i)}=-2\hat{n}\times\vec{E}_t^{\mathrm{II}-(i)}. \tag{14}$$

The electric and magnetic vector potentials can be defined by using the equivalent currents as [10]:

$$\vec{F}=\frac{\epsilon_1}{4\pi}\int_S\overrightarrow{M_s}(x',y',z')\frac{e^{-jk_1R}}{R}ds', \tag{15}$$

$$\vec{A}=\frac{\mu_1}{4\pi}\int_S\overrightarrow{J_s}(x',y',z')\frac{e^{-jk_1R}}{R}ds', \tag{16}$$

where R represents the distance from any point of the source to the observed point. The radiation fields in far-field are

$$\begin{aligned}H_r\approx 0 H_\theta&\approx\frac{jk_1e^{-jk_1r}}{4\pi r}\left(N_\phi-\frac{L_\theta}{\eta_1}\right)\\H_\phi&\approx-\frac{jk_1e^{-jk_1r}}{4\pi r}\left(N_\theta+\frac{L_\phi}{\eta_1}\right),\end{aligned} \tag{17}$$

where $\eta_1=\sqrt{\mu_1/\epsilon_1}$ and

$$N_\theta=\iint_S J_x\cos\theta\cos\phi\, e^{jk_1r'cos\psi}ds', \tag{18}$$

$$N_\phi=\iint_S -J_x\sin\phi\, e^{jk_1r'cos\psi}ds', \tag{19}$$

$$L_\theta=\iint_S M_y\cos\theta\sin\phi e^{jk_1r'cos\psi}ds', \tag{20}$$

$$L_{\phi} = \iint_{S} M_y \cos\phi \, e^{jk_1 r' cos\psi} ds'. \tag{21}$$

We can evaluate the total far-field scattered field which is equal to the numerator in (12) by using (17) and vector transformation.

Before jumping into numerical results, it is important to point out how the SPP-like resonance frequency is decided. However, our formulation makes it difficult to derive the frequency through the parameters, such as a width, a depth, and a period, due to its aperiodicity. Note that previous studies on the periodic grooves provided a relationship between the resonance frequency and the parameters based on Floquet's theorem [6–8, 22, 23]. The general conditions for the excitation of the SPP-like modes in terms of wavelength are $p \approx \lambda$ and $d \approx (2n+1)\lambda/4$, where p is a period of the grooves and d is a depth of the grooves. We started to design the modulated grooves under these conditions.

As can be seen from Fig. 1, relatively small grooves ($i = 2, 3, 5, 7, 8, 10, 12, 13, 15, 17, 18$) have a period 20 mm, $T^{(2)} = -100$ mm, a depth $d^{(i)} = 4$ mm, and a width $2w^{(i)} = 1.2$ mm, all of which are aimed at the excitation of the SPP-like modes at one frequency, whereas the other grooves ($i = 1, 4, 6, 9, 11, 14, 16, 19$) have a period 30 mm, $T^{(1)} = -105$ mm, a depth $d^{(i)} = 6$ mm, and a width $2w^{(i)} = 4$ mm for the other frequency. The total number of grooves is $N = 19$ and that the number of small and large grooves is 11 and 8, respectively. All regions are assumed to be filled with air. The periodic small grooves can generate the SPP-like modes at about 13.8 GHz as described in [7], whereas the others can generate the SPP-like modes at about 8.3 GHz. Before proceeding with the investigation of dual band RCS reduction due to the SPP-like modes, it is pertinent to validate our mode matching formulation. Toward this purpose, our bistatic RCS results are compared with the simulation results from MWS of CST and FEKO in Fig. 2. Note that bistatic RCS of an infinite rectangular conducting plane becomes non-finite, and thus we assume that the sizeof the proposed structure is 1 m × 1 m in length and width throughout the analysis. The comparison of our results with the simulation results shows a good agreement at both frequencies. For the mode matching method, the total computation time with the truncation number $M = 4$ is about 20 s on a PC (Intel Core CPU i7-5820 k at 3.30 GHz, 32 GB memory).

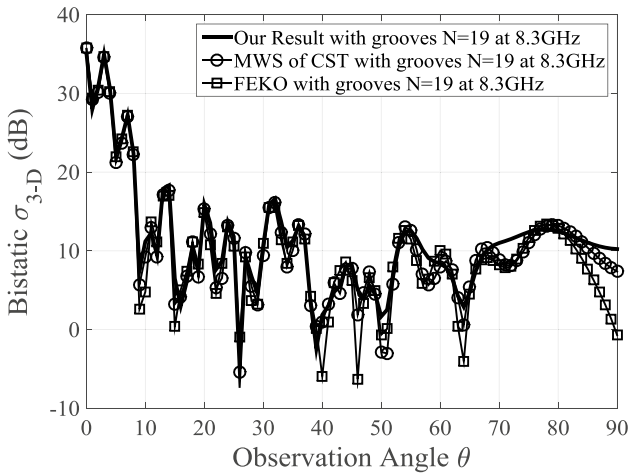

Fig. 2 **a** Bistatic RCS of the modulated grooves in a conducting plane when an incident plane wave is normally incident on the surface at 8.3 GHz and **b** corresponding bistatic RCS at 13.8 GHz ($\phi = 0°$)

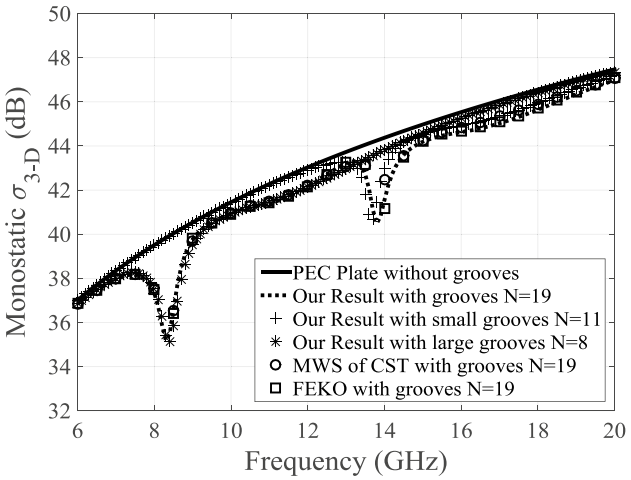

Fig. 3 Monostatic RCS of the modulated grooves in a conducting plane versus frequency when an incident plane wave is normally incident on the surface in the cases of a smooth conducting plane, a plane with both small and large grooves, with either small or large grooves, and simulations of MWS of CST and FEKO

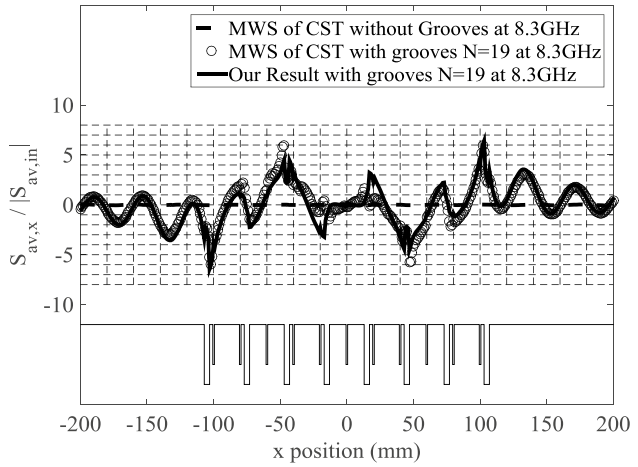

Fig. 4 Ratio of the time-averaged Poynting vector toward x-direction near the conductor surface ($z = 0.5$ mm) to the total magnitude of the time-averaged Poynting vector for a normal incidence plane wave

The total simulation times for MWS of CST and FEKO on the same PC are over 1.5 h and about 6 min, respectively, implying that our computational method is more efficient for the optimization of the structure. The discrepancy in large observation angles toward 90 degrees is due to the diffraction of edges. Figure 3 illustrates the monostatic RCS results in the case of normal incidence ($\theta_i = \theta_s = 0°$) from 6 GHz to 20 GHz under various conditions. As is known, the monostatic RCS increases as the frequency increases. To verify aforementioned statements that the periodic small grooves are designed for 13.8 GHz and the other periodic large grooves are for 8.3 GHz, we plot the results using only small grooves ($N = 11$) or large grooves ($N = 8$) on the conducting plane. Compared to monostatic RCS of the conducting plane without grooves, the result of the corresponding plane with only small grooves shows the reduction of monostatic RCS at 13.8 GHz. Also, the result of the corresponding plane with only large grooves shows the reduction of monostatic RCS at 8.3 GHz. From these results, each of the periodic grooves excites the SPP-like modes at the desired frequency and the presence of the SPP-like modes reduces the reflection in terms of monostatic RCS. Also, it is interesting that the proposed structure including both groups of small and large grooves results in the reduction of monostatic RCS over two targeted frequencies. Therefore, the reduction of monostatic RCS can be achieved due to the excitation of the SPP-like modes at both frequencies.

In order to assure the existence of the SPP-like modes, we calculate the ratio of the time-averaged Poynting vector toward x-direction $S_{av-x}(x, z)$ near the interface ($z = 0.5$ mm) to the total magnitude of the time-averaged Poynting vector of the incident plane wave $\left|S_{av-in}(x, z)\right|$ at 8.3 GHz and compare our result with simulation result of MWS of CST, as shown in Fig. 4. The comparison of our result with the simulation result shows a good agreement. Compared to the time-averaged Poynting vector in the case of the conducting plane without grooves, the time-averaged Poynting vector in the case of corresponding plane with modulated grooves in non-zero, even has larger values. This means the presence of the SPP-like modes propagating along the interface, thereby making the reduction of reflection.

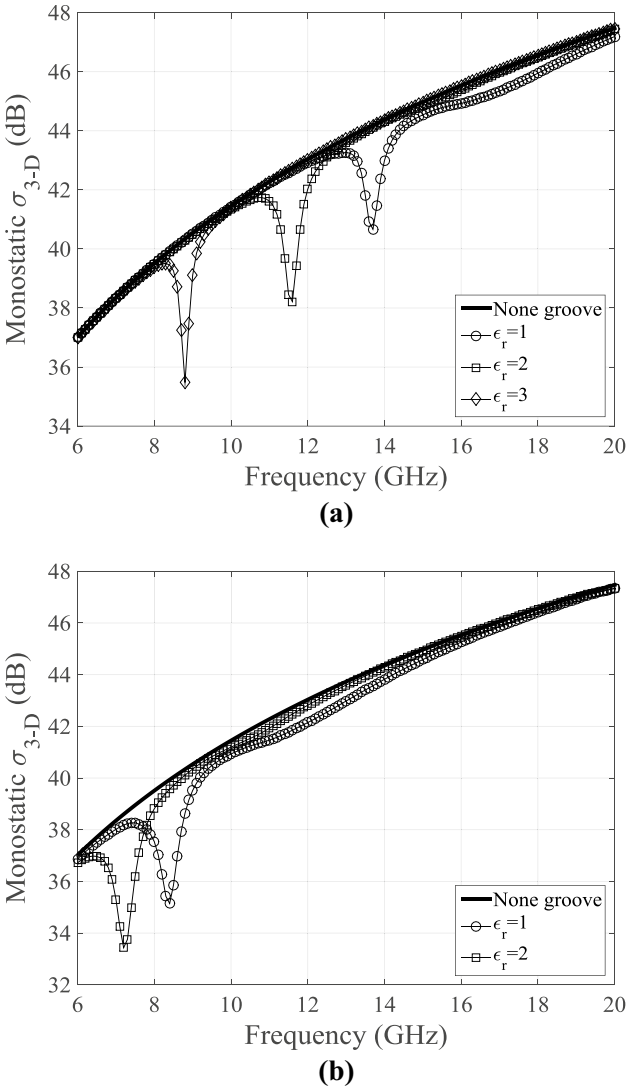

Fig. 5 Monostatic RCS versus frequency as dielectric constant varies in cases of the rectangular conducting plane with **a** relatively small grooves only ($N = 11$) and **b** large grooves only ($N = 8$) ($\phi = 0°$, $\theta = 0°$)

Effects of dielectric filled grooves in a rectangular conducting plane are also analyzed. The effects on electromagnetic scattering are plotted, given that dielectric constant is finite, real value, as shown in Fig. 5. Figure 5a shows monostatic RCS as dielectric constant varies in the case of the rectangular conducting plane with relatively small

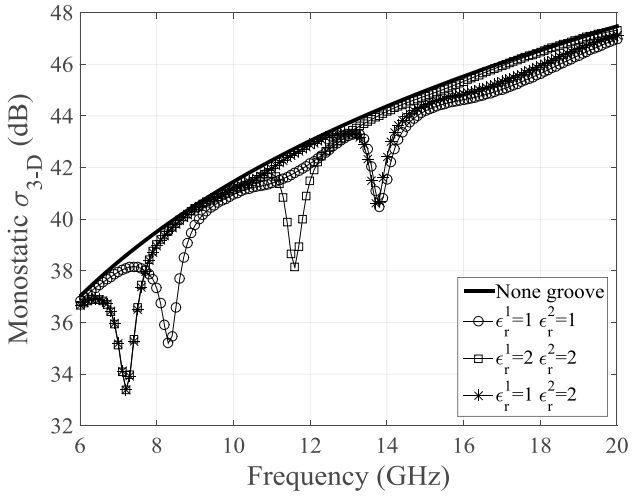

Fig. 6 Monostatic RCS of the modulated grooves filled with dielectrics versus frequency ($\phi = 0°, \theta = 0°$)

grooves ($N = 11$), whereas Fig. 5b shows corresponding result when the surface of the conducting plane consists of relatively large grooves ($N = 8$). As can be seen, the SPP-like resonance frequency decreases as the dielectric constant increases in both cases. Large dielectric constant seems to give rise to the decrease of the asymptotic SPP-like resonance frequency, and therefore the intercept point for phase matching between the incident wave and the SPP-like modes is positioned at low frequency in terms of the dispersion relation. Similar to the former result that shows the feasibility of dual band RCS reduction by combining arrays of grooves designed for different frequencies, monostatic RCS of combined arrays of grooves with dielectric constant more than 1 is plotted in Fig. 6. Superscript 1 in the legend denotes relatively small grooves and 2 represents the other grooves. We extrapolated from Fig. 6 that each array of grooves filled with dielectric excites the SPP-like modes independently. Also, we can modify the resonance frequency via dielectrics.

4 Conclusion

We have solved the electromagnetic boundary-value problem of the modulated grooves in an infinite conducting plane based on the Fourier transform, eigenfunction expansion, and mode matching method. RCS is represented in the series form and calculated in terms of the groove geometry to analyze the characteristics of dual band RCS reduction. As a result, due to the excitation of the SPP-like modes, monostatic RCS can be reduced at dual band. Our formulation and results can be used in the research of RCS reduction and stealth technology.

Acknowledgements This research was partly supported by Basic Science Research Program through the National Research Foundation of Korea (NRF) funded by the Ministry of Science and ICT (No. 2017R1A2B4001903) and ICT & R&D program of MSIP/IITP [No. 2016-0-00130, Cloud based SW platform development for RF design and EM analysis] and the Basic Science Research Program through the National Research Foundation of Korea (NRF) funded by the Ministry of Education (No. 2015R1A6A1A03031833).

References

1. Oliner AA, Jackson DR (2003) Leaky surface-plasmon theory for dramatically enhanced transmission through a subwavelength aperture, part I: basic features. In: Proc. IEEE Antennas Propag. Soc. Int. Symp. , pp. 1091–1094
2. Jackson DR, Zhao T, Williams JT, Oliner AA (2003) Leaky surface-plasmon theory for dramatically enhanced transmission through a sub-wavelength aperture, part II: leaky-wave antenna model. In: Proc. IEEE Antennas Propag. Soc. Int. Symp, pp. 1095–1098
3. Martín-Moreno L, García-Vidal FJ, Lezec HJ, Degiron A, Ebbesen TW (2003) Theory of highly directional emission from a single subwavelength aperture surrounded by surface corrugations. Phys Rev Lett 90:167401
4. García-Vidal FJ, Martín-Moreno L, Lezec HJ, Ebbesen TW (2003) Focusing light with a single subwavelength aperture flanked by surface corrugations. Appl Phys Lett 83(22):4500–4502
5. Degiron A, Ebbesen TW (2004) Analysis of the transmission process through single apertures surrounded by periodic corrugations. Opt Express 12(16):3694–3700
6. García-Vidal FJ, Martín-Moreno L (2002) Transmission and focusing of light in one-dimensional periodically nanostructured metals. Phys Rev B 66:155412
7. Na DY, Kim JH, Park YB, Jung K-Y (2013) Enhanced and directional transmission through a slit surrounded with grooves in a conducting plane. IET Microw Antennas Propag 7(10):843–850
8. García-Vidal FJ, Martín-Moreno L, Pendry JB (2005) Surfaces with holes in them: new plasmonic metamaterials. J Opt A Pure Appl Opt 7(2):S97
9. Pendry JB, Martín-Moreno L, García-Vidal FJ (2004) Mimicking surface plasmons with structured surfaces. Science 305:847–848
10. Balanis CA (2012) Advanced engineering electromagnetics, 2nd edn. Wiley & Sons Inc, New York, pp 328–333
11. Liang W et al (2012) Anomalous microwave reflection from a metal surface induced by spoof surface plasmon. Chinese Phys B 21(1):017301
12. Park TJ, Eom HJ (1993) An analysis of transverse electric scattering from a rectangular channel in a conducting plane. Radio Sci 28(5):663–673
13. Barkeshli K, Volakis JL (1991) Scattering from narrow rectangular filled grooves. IEEE Trans Antennas Propag 39(6):804–810
14. Cho YH (2006) TM plane-wave scattering from finite rectangular grooves in a conducting plane using overlapping T-block method. IEEE Trans Antennas Propag 54(2):746–749
15. Gao X et al (2012) Dual-band spoof surface plasmon polaritons based on composite-periodic gratings. J Phys D Appl Phys 45(50):505104

16. Lee IG, Yoon SH, Lee JS, Hong IP (2016) Design of wideband radar absorbing material with improved optical transmittance by using printed metal-mesh. Electron Lett 52(7):555–557
17. Shin H et al (2017) Analysis of radar cross section of a battleship equipped with an integrated mast module based on PO and PTD. J Electromagn Eng Sci 17(4):238–240
18. Ha J et al (2017) Effect of plasma area on frequency of monostatic radar cross section reduction. J Electromagn Eng Sci 17(3):153–158
19. Lee JH et al (2018) Attenuation effects of plasma on Ka-band wave propagation in various gas and pressure environments. J Electromagn Eng Sci 18(1):63–69
20. Kim Y et al (2018) Numerical investigation of scattering from a surface dielectric barrier discharge actuator under atmospheric pressure. J Electromagn Eng Sci 18(1):52–57
21. Harrington RF (2001) Time-harmonic electromagnetic fields, 2nd edn. Wiley, New York, pp 143–145
22. López-Rios T et al (1998) Surface shape resonances in lamellar metallic gratings. Phys Rev Lett 81(3):665–668
23. Beruete M et al (2004) Enhanced microwave transmission and beaming using a subwavelength slot in corrugated plate. IEEE Antennas Wirel Propag Lett 3:328–331

Sangsu Lee received B.S. degree in the department of Electrical and Computer Engineering from the Ajou University, Suwon, Rep. of Korea, in 2017. He is currently working on M.S. course in the department of Electrical and Computer Engineering, Ajou University, Suwon, Rep. of Korea. His research interests include electromagnetic field scattering analysis, metamaterials, metasurfaces, and plasmonics.

Heejae Jun received B.S. and M.S. degree in the department of Electrical and Computer Engineering from the Ajou University, Suwon, Rep. of Korea, in 2016 and 2018, respectively. He is currently with MOASOFT Corporation. His research interests include electromagnetic field scattering analysis and metamaterial antennas.

Kyung-Young Jung received B.S. and M.S. degrees in Electrical Engineering from Hanyang University, Seoul, Korea in 1996 and 1998, respectively and a Ph.D. degree in Electrical and Computer Engineering from The Ohio State University, Columbus, Ohio in 2008. From 2008 to 2009, he was a postdoctoral researcher at The Ohio State University, and from 2009 to 2010, he was an Assistant Professor with the Department of Electrical and Computer Engineering, Ajou University, Korea. Since 2011, he has worked at Hanyang University, where he is now an Associate Professor in the Department of Electronic Engineering. His current research interests include computational electromagnetics, bio electromagnetics, and nano electromagnetics.

Hosung Jung Choo received his B.S. degree in Radio Science and Engineering from Hanyang University, Seoul in 1998 and his M.S. and Ph.D. degrees in Electrical and Computer Engineering from the University of Texas at Austin in 2000 and 2003, respectively. In September 2003, he joined the School of Electronic and Electrical Engineering in Hongik University, Seoul, Korea, where he is currently a professor. His principal area of research includes electrically small antennas for wireless communications, reader and tag antennas for RFID, on-glass and conformal antennas for vehicles and aircraft, and array antennas for GPS applications.

Ic-Pyo Hong received the B.S., M.S., and Ph.D. degrees in electronics engineering from Yonsei University, Seoul, South Korea, in 1994, 1996, and 2000, respectively. From 2000 to 2003, he was with the Information and Communication Division, Samsung Electronics Company, Suwon, South Korea, where he was a Senior Engineer with CDMA Mobile Research. Since March 2003, he has been with the Department of Information and Communication Engineering, KongJu National University, Cheonan, South Korea, where he is currently a Professor. In 2006 and 2012, he was a Visiting Scholar at Texas A&M University, College Station, TX, USA, and Syracuse University, Syracuse, NY, USA, respectively. His research interests include numerical techniques in electromagnetics and periodic electromagnetic structures.

Bae Park received B.S., M.S., and Ph.D. degrees in electrical engineering from the Korea Advanced Institute of Science and Technology, South Korea, in 1998, 2000, and 2003, respectively. From 2003 to 2006, he was with the Korea Telecom Laboratory, Seoul, South Korea. In 2006, he joined the School of Electrical and Computer Engineering, Ajou University, South Korea, where he is now a Professor. His research interests include electromagnetic field analysis and electromagnetic interference and compatibility.